Dynamic modelling of biomass power plant using micro gas turbine

S. Barsali*, A. De Marco[1], R. Giglioli, G. Ludovici, A. Possenti[1]
DESTEC, University of Pisa
Largo Lucio Lazzarino, I-56122, Pisa, Italy
*tel +390502217320, fax +390502217333, e-mail stefano.barsali@unipi.it

Abstract

Biomass is becoming a more and more interesting option to replace conventional fossil fuels for heat and power generation. Small plants able to use solid biomass, collected in the plant neighbourhoods, are having a growing diffusion: University of Pisa jointly with some local manufactures has designed, built and tested an externally fired micro gas turbine (EFMGT) supplying 70 kW of electricity as well as 200-250 kW of useful heat. The present paper focuses on the development of a dynamic simulator of the plant. A mathematical model was implemented for the physical and chemical behaviour of the biomass combustion process, as well as for heat transfer mechanisms and turbine behaviour to assess the plant operating variables in both steady state and transient operating conditions. Comparison between model results and data gathered on a test plant shows a good matching (with deviation below 5%) of the main and most critical variables in a wide range of operating conditions which makes the model suitable for synthesize a closed-loop control system able to ensure the highest performances in power production.

Keywords

Externally Fired Micro Gas Turbine (EFMGT), Solid biomass, Combined Heat and Power, Combustion, Modelling

Nomenclature

ACRONIMOUS

EFMGT:	Externally Fired Micro Gas Turbine;
HHV:	Higher Heating Value;
HV:	Heating Value;
ORC:	Organic Rankine Cycle;

SYMBOLS

A:	pre-exponential factor for the Arrhenius-type kinetic rate law [1/s];
a:	exponent for carbon monoxide rate law;

[1] A. De Marco and A. Possenti participated as consultant of the University of Pisa

A_0: pre-exponential factor for carbon monoxide rate law [$sec^{-1}\cdot(mol/cm^3)^{-(a+b)}$];

A_p: particle surface [m^2];

B: activation energy for carbon monoxide rate law [cal/mol];

b: exponent for carbon monoxide rate law;

c_p: specific heat at constant pressure [kJ/(kg·K)];

c_v: specific heat at constant volume [kJ/(kg·K)];

D_0: parameter describing the characteristics of the compressor [m];

D_p: diameter of the particle [m];

E: activation energy for the Arrhenius-type kinetic rate law [J/kg];

f: mass of a considered compound over the total dry mass of biomass;

g: mass flow rate [kg/s];

h: specific enthalpy [kJ/kg];

H_{EV}: latent heat of vaporization [kJ/kg];

HV: Heating Value [kJ/kg];

h_m: mass transport coefficient [$kg/(m^2\cdot s\cdot Pa)$];

k: kinetic constant for a volatile rate law [1/s];

K_C: combustion rate coefficient [$kg/(m^2\cdot s\cdot Pa)$];

K_t: turbine constant [$kg\cdot K^{0.5}/(s\cdot Pa)$];

L: length of the edge of the cell [m];

l_p: height of the particle [m];

M: mass [kg];

n_p: number of particles;

P pressure [Pa]

P_{O2}: partial pressure of the O_2 [Pa];

Q: thermal power;

q: volumetric flow rate [m^3/s];

R: gas constant [J/(kg·K)];

r: pressure ratio;

Re: Reynolds number;

S_{att}: active surface of the cell [m^2];

S: surface of the cell [m^2];

63 T: temperature [K];
64 t: time [s];
65 V: volume [m^3];
66 V_0: velocity [m/s];
67 W: power (kW);
68 Y: concentration of volatile component [mol/cm^3];
69 Γ: convective heat transfer coefficient [kW/(m^2·K)];
70 γ: specific heat ratio;
71 ε: void fraction;
72 η: efficiency;
73 λ: conduction heat transfer coefficient [kW/(m·K)];
74 λ_{Gas_RAD}: radiation heat transfer coefficient [kW/(m^2·K^4)];
75 μ: kinematic viscosity [kg/(m·s)];
76 ρ: average density in a cell [kg/m^3];
77 Φ: flow number [1/s];
78 ω: rotational speed of the turbine [1/s];
79 [*i-th*] concentration of the *i-th* component [mol/cm^3];
80
81 *SUBSCRIPT*
82 *a:* process air;
83 *amb*: ambient;
84 *bio*: biomass;
85 *C*: char compound;
86 *c*: compressor;
87 *cr*: critical;
88 *CO*: carbon monoxide compound;
89 *COND*: conduction;
90 *E*: east cardinal point;
91 *EV*: evaporation process;
92 *e*: expansion;
93 *ex*: exhaust;
94 *Gas*: gaseous compounds composed by the combustion air and combustion products;
95 *GEN*: gaseous compounds composed by combustion products;

H2: hydrogen compound;
H2O: water;
in: incoming compound in the cell;
RAD: radiation;
m: metal;
mec: mechanical;
n: nominal;
N: north, cardinal point;
out: outgoing compound from the cell;
r: request;
ref: reference;
S: south, cardinal point;
Sol: solid biomass;
t: turbine;
tot: total;
vli: *i-th* volatile;
W: H_2O due to the moisture content in the solid biomass;
We: west, cardinal point;

1 Introduction

In recent years, biomass has gained a growing interest for electricity generation due to the increased diffusion of renewable sources [1], particularly due to the possible usage of some residues (i.e. organic wastes, scraps of woods or pruning etc.) which can not be exploited for other manufacturing processes. Unlike wind and solar energy, biomass is a storable and programmable source which can be used to meet a wide range of energy needs, using different energy conversion technologies [2]; particular attention concerns biomass utilization in electricity and heat production.

Today, only medium and large scale plants are able to directly use solid biomass for commercial electricity generation. Usually, steam turbines are coupled to biomass fired boilers. A different approach is to process the fuel through chemical reactions (gasification, pyrolysis) in large conversion plants to obtain a gaseous or liquid fuel to be used in reciprocating engines.

All these solutions need a minimum economical size which corresponds to electricity generation above some hundred kilowatts. Also plants for chemical treatments need a rather large size. As a consequence, the logistics aspects for biomass collection, storage and delivery might have a significant impact on the economic and environmental costs of a project.

Small plants, able to directly use solid biomasses collected in the plant neighbourhoods, have the chance to overcome these drawbacks.

Gas turbines can be used only through an external heat generator where the biomass is burnt for heating the air of the primary Brayton cycle, through a high temperature heat exchanger.

According to theoretical studies [3], [4] an externally fired micro gas turbine has the opportunity of reaching electrical efficiency higher than the other technological choices.

University of Pisa together with some local manufacturers, has designed, built and tested an externally fired micro gas turbine (EFMGT) supplying 70 kW of electricity as well as 200-250 kW of useful heat. When heat can not be usefully exploited, a solution has been built to recover it by an ORC system for additional electricity generation (30 kW) [5], [6].

Control and operation of this kind of plants is a challenging task, due to the large number of parameters and variables affecting the system behaviour and to highly non-linear phenomena which govern its response.

Simulation, therefore, is an essential tool to understand the physical mechanisms regulating the dynamic responses of the system due to changes of the operating parameters and external conditions. As a consequence, a simulator is very useful to synthesize a suitable closed-loop control system, which ensures the prompt response to external parameters and to generation request, while keeping the highest possible performance. Biomass power plant performances are very sensitive to the quality of the fuel: any change regarding composition and moisture content, that may occur during the plant operation, deeply affects its power production. Controlling mass and combustion air flows is essential to ensure the best and continuous plant performances as well as to increase the plant life length.

A dynamic simulator, based on mass and energy balances for each element of the system, has thus been developed in order to reproduce the plant behaviour during the start-up, regime and shut-off phases or following some disturbances. The simulator is aimed to provide a realistic behaviour of the physical system without giving a too detailed description which would require the integration of computational fluid-dynamics finite element modelling with time domain simulations, getting to unacceptable calculation tool requirements.

Dynamic simulation plays a key role in the design of the control system of thermal power generation plants, in particular when innovative design solutions are adopted. There is a long track of research and engineering effort in this field [7 - 12].

Several tools have been developed in order to simulate the dynamic behaviour of a thermo-electric power plant based on solid biomass conversion [13], [14]. They usually describe the combustion chamber as interpolatory time dependent functions with known values of the time constants,

obtained on the basis of experimental data. In this case, the influence of the disturbances in the combustion process and consequently in power production is not considered.

On the other hand, CFD commercial software are able to provide detailed analysis of the thermo-fluid dynamic field in the combustion chamber, also considering the main chemical reactions regarding the gaseous species involved in the combustion process. Usually the solid biomass combustion process is not considered in CFD codes, hence it is generally implemented in specific UDF (User Defined Function) [15], [16], [17].

The inability to study the whole dynamic evolution of a system as a consequence of a disturbance and the lack of the characterization of the solid combustion process are the main limits for a CFD codes utilization.

Other commercial software packages can be able to reproduce dynamic behaviour of thermo-electric plants basing on models of physical processes as combustion, but they often suffer from being opaque: the equations actually used are unknown and incorporating a specific know-how could be very hard [18], as for CFD software.

Conversely many codes have been developed by individual users which have the full control of the equations implemented in the system [9].

The simulator developed in this work, in particular, includes a physical (although basic) model of the combustion process. A spatial, as well as temporal, description of the main physical and chemical phenomena of biomass combustion was introduced, in order to have a basic knowledge regarding the evolution of the gas flow and the solid consumption, due to the chemical reactions and heat transfer mechanisms.

In conclusion, the simulator combines the modelling approach, oriented to provide reliable system behaviour representation on the basis of the combustion and heat exchange processes, with the modelling approach oriented to system control issues. The simulator can, also, be easily adapted to model different kinds of power plants using solid fuel for energy production by rearranging the basic blocks describing the main phenomena. A first application of the model is presented in this work for checking a possible closed loop control system.

2 Externally fired micro gas turbine plants

The key factor which makes a small biomass plant able to compete with other solutions in the market is the possibility of exploiting small amounts of solid biomass which can be collected in the neighborhood of the plant with low logistic costs and without any complex fuel processing treatment such as gasification or pyrolysis.

2.1 Reference plant layout

Starting from some commercial micro gas turbines (in the size of some tens of kW), and replacing the gas burners with an external biomass heat generator, the University of Pisa jointly with some local manufacturers, as reported above, has built a Combined Heat and Power plant based on an externally fired micro gas turbine (EFMGT) supplying 70 kW of electricity as well as 200-250 kW of useful heat.

Details of this plant in some applications with different options for fuel supply are described in previous works [5], [6], [19]. Figure 1 shows the layout of the plants developed and the picture of one plant installed and operating at an industrial user.

In some cases, heat can not be usefully exploited in the neighbourhoods of the plant, while electricity from biomass is strongly subsidized in several European electricity markets. This makes the chance to improve the electricity generation, at the expense of heat generation, an attractive perspective. The heat available is enough for generating up to 30kW through an Organic Rankine Cycle system which has been added in some applications. In this work, it is only considered simply as a converter of the energy available in the exhausts into electricity with a linear dependence on the exhaust temperature and including a first order time constant. Its detailed behavior and its characteristics are outside the scope of our work.

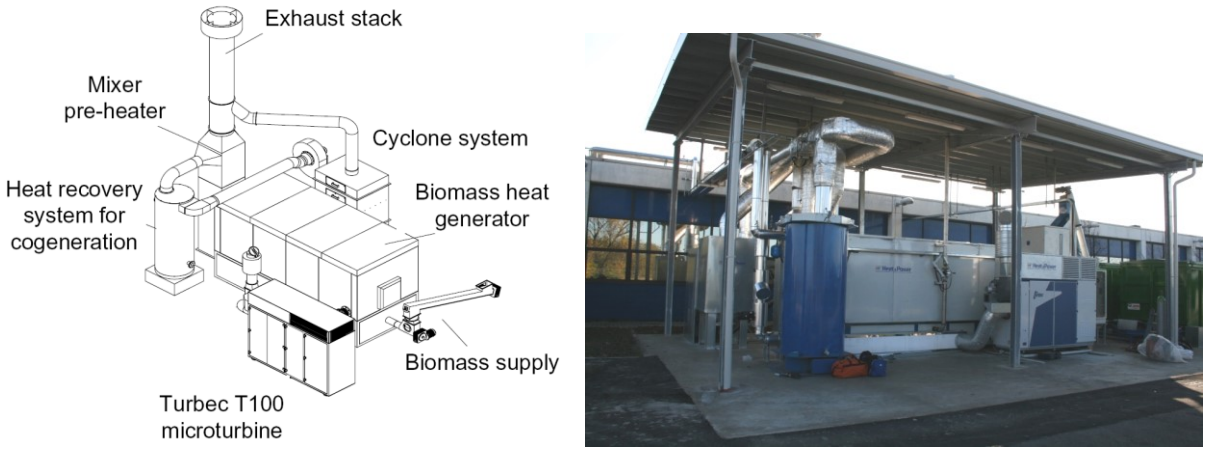

Figure 1: One of the plants in service at an industrial user.

2.2 The EFMGT cycle

The EFMGT system (see figure 2) is mainly composed of a micro-turbine connected to some heat exchangers in a regenerative Brayton cycle using clean air as process fluid. The usual burners of the standard gas-fired micro-turbine are replaced by a high temperature heat exchanger for heating the process air from the biomass combustion.

Biomass is supplied to the heat generator through a screw conveyor, which is designed for the majority of solid biomasses and which introduces the biomass in the lowest zone of the combustion

chamber. Different options have been used for storing and conveying the biomass as described in previous works [5].

The combustion air and process air are fully decoupled. The process air is pressurized by a centrifugal compressor, directly connected to the turbine shaft, and forced into the regenerative heat exchanger before flowing in the high temperature heat exchanger inside the biomass fired heat generator. After crossing the turbine, the expanded, but still hot, air flows into the regenerative heat exchanger (recuperator) for warming the compressed clean air.

External air enters both in the micro-turbine and in the heat generator. The exhaust flow is the sum of these two contributions.

The output air is then mixed with the combustion exhausts to be directly used for thermal applications, or to warm some water (either pressurised or not) which, in turns, can be exploited for thermal use or to supply an Organic Rankine cycle.

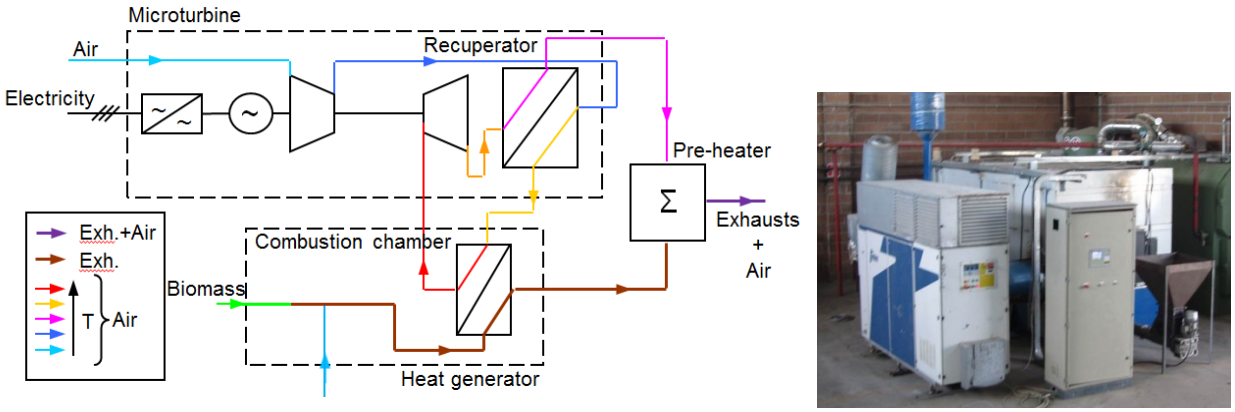

Figure 2: The principle scheme of the EFMGT and the plant at the test facility.

3 Physical approach in system modelling.

The simulation software is based on a mathematical modeling of the physical processes and mechanisms that involve each element of the system. Despite the uncertainty of some physical parameters (i.e. the kinetic constant and temperature values which describe the volatile release from the biomass, the coefficients which describe the chemical oxidation reaction of CO into CO_2, the parameters which describe the char oxidation into CO or CO_2, the fluid-dynamic parameters defining the movement of gases through the porous mass of the biomass), which are very hard to be measured, physical principles are the basis of the simulator, ensuring a plausible behavior of the system even when some parameters values are uncertain. The main parameters have been tuned using data gathered from steady state operation at rated conditions when temperature measurements at different points are available. The so tuned model has then been tested in dynamic operation when only few measurements are available.

It has then be used to check a possible structure of a closed loop control system able to automatically cope with changes of external parameters such as the characteristic of the biomass or the power request.

The model structure is composed by the six blocks that represent the main elements of the plant:

- heat generator;
- micro-turbine;
- gas-air heat exchanger;
- recuperator;
- pre-heater;
- ORC system.

The simulator is implemented on Matlab-Simulink® platform which allows both a dynamic and a stationary study of the system behavior. It is a parametric model, suitable for other systems based on the same principles.

The modeling approach used for the standard components (compressor, turbine and heat exchangers) is based on models already available in the literature [12]. For the heat generator a different approach is used, it implies a spatial and temporal description of the main combustion processes. The dynamic behavior of the system is greatly affected by combustion; for this reason a more detailed description of the physical phenomena inside the combustor is needed to achieve reliable dynamic results. In fact the dynamic behavior of the processes in the combustion chamber depends upon the mechanical movement of the amount of biomass inside, its thermal behavior, the process of moisture and volatile release as well as upon the chemical kinetic of the oxidation reactions. Then the heat stored in the structures of the chamber itself (walls, heat exchanger tubes) introduces further dynamic elements which need to be described.

4 The heat generator: hypotheses and model

The combustor geometry was represented as a parallelepiped (figure 3), in contact with the gas-air heat exchanger (a beam of tubes through which clean air coming from the recuperator flows before the expansion). The combustor can be divided in two parts:

- In the front part of the parallelepiped (combustion chamber), solid biomass reactions occurs and radiation is the main heat transfer mechanism between gases and air in the heat exchanger;
- in the back part, the convection is the main heat transfer mechanism.

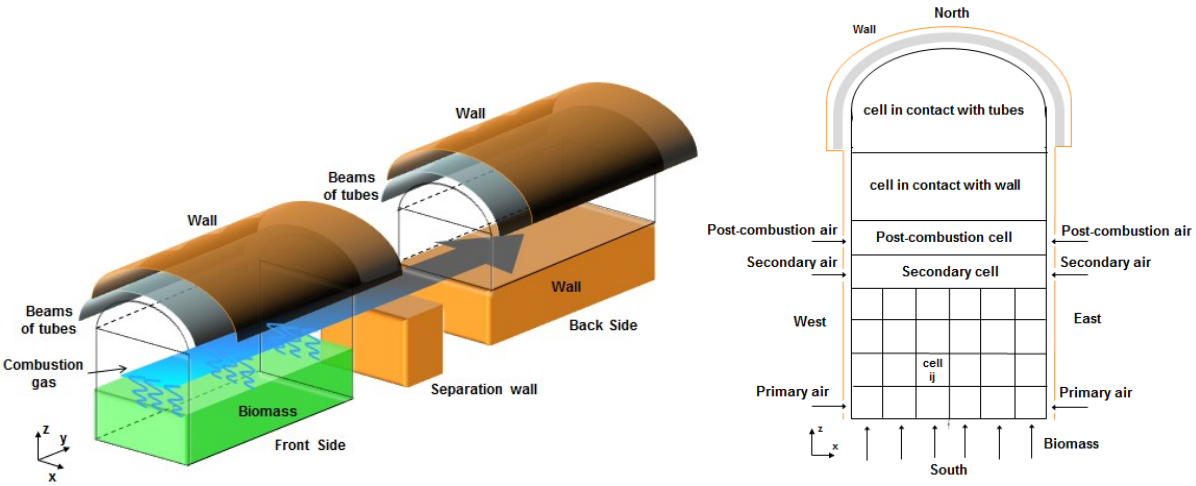

Figure 3: The geometric model of the combustor.

Biomass is fed in the combustion chamber from the bottom: the distribution of solid, as well as the velocity of the gas, can be considered uniform along the y axis. Different solutions using grates can be adopted. The combustion model can be easily adapted by choosing a suitable geometrical configuration of the control volumes, but keeping the same equations which describe the evaporation, volatile release and combustion process, as well as the mass and energy transfer among the control volumes.

A slight negative pressure moves the combustion gases towards the back of the combustor before going out to the pre-heater and the exhaust stack. This movement along y is mainly located around the exchanger pipes, it can be neglected in the zone where the combustion reactions develop.

Under this hypothesis, the problem could be reduced in the x-z plane, where biomass moves only in z direction; all the combustion air flows on x-z planes also in the porous biomass. So all the cells are long as the whole section of the chamber (front side or back side in figure 3)

The cross section of the combustor is divided into a number of control volumes (cells) of significant size in order to spatially describe the main combustion processes without requiring high computational resources. The number of cells is higher in the bottom part of the cross section of the combustor, where solid combustion processes occurs, than in the top part where the chemical reactions only involve gaseous species (the cells have a cross section of 8x7.5 cm in the lower part where the solid biomass is present, 50x7.5 cm for the secondary cell, 150x30 cm for the post-combustion cell and 150x120 cm for the sum of the two cells in contact with tubes and walls; the post combustion and the last two cells are repeated also in the back part of the chamber). During combustion, the boundary of the solid biomass moves from the limit cell where the secondary air is injected to the bottom.

The combustion air is divided on three levels: primary air is blown inside the solid biomass in the lower part of the chamber; secondary air, injected above the biomass surface, is used to complete

chemical reactions on unburned gases. Finally the post-combustion air is used to dilute the exhaust gases and consequently to decrease the concentration of combustions products and control the temperature. Since no solid biomass reaches these zones, just one cell (secondary and post-combustion cell in figure 3, right side) is used to model each zone.

Over the post-combustion cell, the volume of the combustor is divided into two cells: the low one in contact with the insulating wall of the combustor, the high cell in contact with the tubes of the gas-air heat exchanger (figure 3, right side). Radiation and convection are the main mechanisms of heat transfer between wall/tubes and combustion gas in these cells; also the same mechanisms are involved in the heat transfer between wall and tubes. Moreover it is supposed that some oxidation reactions of some residual volatiles can occur in these cells and in the back side of the combustor (figure 3, left side).

4.1 Biomass model: chemical composition and geometry.

The woody biomass species (coming from wood maintenance, residues from wood industry, wood chip or pellet), that can be used in the combined cycle plant, are mainly composed by polysaccharides (cellulose and hemicellulose), and lignin. Glucose ($C_6H_{12}O_6$) can be considered the main element of the "equivalent" biomass used in the simulator. Different composition of the biomass affects the overall behaviour only slightly. It is recognized in literature that this kind of approximation matches the energetic behavior of the biomass, which is the purpose of this work [20, 21, 22]. In case information about pollutant emissions should be assessed, a more detailed analysis is required. Ash has been considered as a percentage of the total mass which does not contribute to the combustion. Since it is just a small percentage of the dry material (below 4%) with the biomass used in the application, it has been included in the solid mass of char to be accounted for in the mass transport phenomena and in the overall density of the material, but does not supply energy.

During combustion, one mole of glucose is decomposed into two moles of carbon (f_C: 133g_C/kg), 4 moles of carbon monoxide (f_{CO}: 622g_{CO}/kg), 2 moles of water (f_{H2O}: 200g_{H2O}/kg) and 4 of hydrogen (f_{H2}: 45g_{H2}/kg) [30]. The HHV of this equivalent biomass made of glucose molecules is about 17000kJ/kg and the LHV 16200kJ/kg, considering the heating value required for carbon, hydrogen and CO oxidation (Table 1) [30]. Although the actual volatiles released change with the biomass used, this equivalent approximation shows a good match with the real behavior for what concerns the energy released during combustion. Condensable tar molecules having high molecular weight can be neglected in this approach for three reasons: first they appear in very low percentage, second, once released they do not condensate in a high temperature combustion chamber, third they are

completely burnt with the excess air available for post combustion. [22, 31, 32], and can, therefore, be assimilated to the other volatiles.

Table 1: Main combustion reaction and their heating values [30].

Chemical Reactions	Heating Value [kJ/kg]
$CO \rightarrow CO_2$	10113
$C \rightarrow CO_2$	32650
$H_2 \rightarrow H_2O$	142800

$$HHV = HV_C \cdot f_C + HV_{CO} \cdot f_{CO} + HV_{H2} \cdot f_{H2} \quad (1)$$

The total mass in a cell is calculated considering the biomass as sum of the following components (2):

- water absorbed by the external environment;
- volatiles divided into CO, H_2 and H_2O, coming from decomposition of glucose during the first phase of combustion;
- char: a carbon residue after the volatilization phase.

Considering the density of each component of the solid, the total density of the solid phase is:

$$\rho_{Sol} = \rho_C + \rho_W + \sum_{i=1}^{3} \rho_{vli} \quad (2)$$

Moreover, the biomass in a cell is considered as a homogenous porous media, composed by a series of pieces, with a parallelepiped shape. The "active" surface of a cell (3) is defined as the boundary surface through which mass and energy exchange occurs during the combustion processes:

$$\mathrm{S}_{\mathrm{att}} = 2 \cdot A_p \cdot n_p \cdot S_N \cdot L_{We} \quad (3)$$

where S_N and L_{We} are respectively the surface and the length normal to North and West directions. n_p is the number of biomass pieces in the cell and it is a function of the void fraction in a cell:

$$n_p = \frac{(1-\varepsilon)}{2 \cdot A_p \cdot l_P} \quad (4)$$

As consequence the volume of the biomass in a cell could be defined as follows:

$$V_{Sol} = 2 \cdot A_p \cdot n_p \cdot S_N \cdot L_{We} \cdot l_P \quad (5)$$

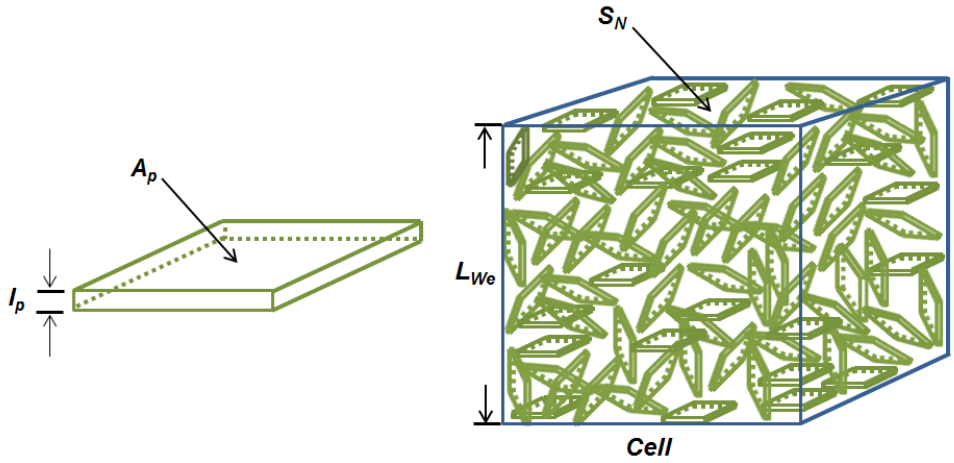

Figure 4: A biomass particle and a cell of the combustion chamber filled with biomass particles.

4.2 Biomass combustion processes

Biomass combustion process is divided into four main phases:

- biomass drying and water evaporation process;
- pyrolysis;
- volatiles oxidation;
- char oxidation.

Combustion is started from the surface layer of solid biomass where the secondary air is injected. The biomass below, initially cold, is warmed by the conduction mechanism and the mass transport through the cells. During the heating process, a share of heat is used for water evaporation process. During pyrolysis, it is supposed that the three main volatile compounds (H_2, CO and H_2O) are released respectively at three different activation temperatures (250°C , 350°C, 550°C) according to the physical mechanism [20, 21, 22]:

$$\frac{dY_i}{dt} = -k_i \cdot Y_i \tag{6}$$

k_i is the kinetic constant, referred to each volatile Y_i, of the Arrhenius-type kinetic rate law:

$$k_i = A_i \cdot \exp(-E_i / RT) \tag{7}$$

We decided to simplify this process to only three species of volatiles to keep the problem complexity within reasonable limits to make it possible modeling the whole plant while saving the physical approach, and gaining a reasonable behavior even with lacking data. Then carbon dioxide and water are produced by the oxidation of H_2 and CO; heat produced by these exothermic reactions, warms gases and the solid biomass (through convection mechanism) in the cell.

Moreover it is supposed that the H_2 immediately reacts with the oxygen in the cell, while the oxidation of CO depends on the reaction kinetics [24], only the remaining oxygen is used for char oxidation.

$$\frac{d[CO]}{dt} = A_0 \exp\left(-\frac{B}{RT}\right)\cdot[CO]\cdot[O_2]^a\cdot[H_2O]^b \qquad (8)$$

where R in this case is 1.987 cal/(K·mol), the parameters A_0 ($1.2\cdot10^{10}$ $sec^{-1}\cdot(mol/cm^3)^{-(a+b)}$), B ($1.6\cdot10^4$ $cal\cdot mol^{-1}$), a (0.3) and b (0.5) are estimated following the Hottel-Williams approximation [23].

The char combustion begins at the ignition temperature of 650°C; after drying and volatilization processes, solid biomass is composed by char and ashes.

During combustion, char oxidation produces CO as a function of the oxygen concentration in the cell, the coefficient of burning rate and the mass transport coefficient as described in (9). If the oxygen concentration is sufficiently high, CO_2 is produced by CO oxidation.

$$g_{CO}(char) = \left(\frac{K_c\cdot h_m}{K_c + h_m}\cdot S_{att}\cdot P_{O2}\right)\cdot\frac{24}{32} \qquad (9)$$

$g_{CO}(char)$ is the mass flow rate of CO due to char oxidation.

The combustion rate coefficient (K_c) is a function of the solid biomass temperature, the mass transport coefficient (h_m) is a function of the Sherwood number, the oxygen diffusivity, the solid biomass temperature and the diameter of the particle [24] [25].

4.3 Main equations of the cell

Mass and energy flows occur through the boundaries of the cells by the convention shown in figure 5, where each side of a cell is named with a cardinal point. The figure also shows the directions assumed as positive reference for each variable.

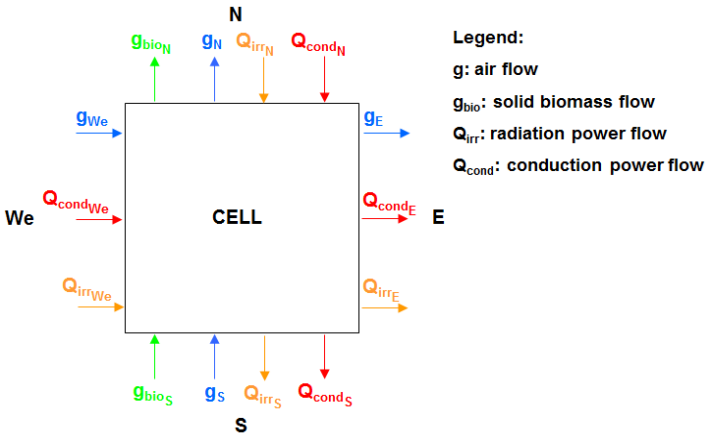

Figure 5: Mass and energy flows through the boundaries of the cell[2].

[2] $g^{bio} = q_{Sol}\cdot\rho_{Sol} = q_{Sol}\cdot\left(\rho_C + \rho_W + \sum_{i=1}^{3}\rho_{vli}\right)$; $Q_{COND} = \lambda\cdot\sum_{i=We,N}\frac{S_i}{L_i}\cdot(T_i - T)$; $Q_{RAD} = \lambda_{Gas\_RAD}\cdot\sum_{i=N,We}S_i\cdot\left(T_{Gas\_i}^{\ 4} - T_{Gas}^{\ 4}\right)$, referred to equation (11).The subscript S and N indicates the entering and exiting fluxes.

Mass and energy conservation equations are the main parts of the structure for each cell. They resume each phase of the combustion process and they differ for solid (10-11) and gaseous components (12-15) in the cell.

Mass conservation in the solid phase is represented by:

$$\left(V_{Sol}\cdot\frac{d\rho_C}{dt}+g_{CO}(char)\right)+\left(V_{Sol}\cdot\frac{d\rho_W}{dt}+g_{EV}\right)+\left(V_{Sol}\cdot\sum_{i=1}^{3}\frac{d\rho_{vli}}{dt}+\sum_{i=1}^{3}g_{vli}\right)= \\ =q_{Sol}\cdot\left(\rho_{C\_S}-\rho_{C\_N}\right)+q_{Sol}\cdot\left(\rho_{W\_S}-\rho_{W\_N}\right)+q_{Sol}\cdot\left(\sum_{i=1}^{3}\rho_{vli\_S}-\sum_{i=1}^{3}\rho_{vli\_N}\right) \tag{10}$$

where the first three terms mass variation due to char combustion and volatile and water release; the second three terms refer to solid mass transfer among cells.

The energy conservation equation (11), states that, in the solid phase, the derivative of temperature with respect to time (11) is a function of mass transport between cells, water evaporation, char combustion, and the heat transfer mechanisms: convection between gas and solid biomass and conduction between biomass in neighboring cells.

$$c_{v\_Sol}\cdot M_{Sol}\frac{dT}{dt}=c_{v\_Sol}\cdot q_{Sol\_S}\cdot\rho_{Sol\_S}\left(T_S-T\right)-g_{EV}\cdot H_{EV} \\ +g_{CO}(char)\cdot HV_{char}+\Gamma_{Gas\_Sol}\cdot S_{att}\cdot\left(T_{Gas}-T\right)+\lambda\cdot\sum_{i=We,N}\frac{S_i}{L_i}\cdot\left(T_i-T\right) \\ -\lambda\cdot\sum_{i=E,S}\frac{S_i}{L_i}\cdot\left(T-T_i\right) \tag{11}$$

where S_i and L_i are the surface and the length of the cell normal to the *i-th* cardinal direction; T is the temperature of solid biomass in the cell and T_i is the temperature of solid biomass in the cells next to the considered one.

Mass conservation equation in the gaseous phase is:

$$g_{GEN}+g_{We}-g_E-g_N+g_S=\frac{V_{Gas}}{RT_{Gas}}\cdot\frac{dP}{dt}-\frac{V_{Gas}\cdot\rho_{Gas}}{T_{Gas}}\cdot\frac{dT_{Gas}}{dt} \tag{12}$$

where g_{We} and g_S are defined by the boundary conditions and g_N e g_E are estimated through the Ergun equation for a fluid in a porous media for transient flow regime (10<Re<1000) [27]: the pressure drop (13) is a function of the void fraction of the cell, the equivalent diameter of the particle and gas velocity , as well as the kinematic viscosity and the density of the fluid:

$$\frac{\Delta P}{L}=150\cdot\left(\frac{\mu_{Gas}\cdot V_0}{D_P^2}\right)\cdot\frac{\left(1-\varepsilon\right)^2}{\varepsilon^3}+\frac{7}{4}\cdot\left(\frac{\rho_{Gas}\cdot V_0^2}{D_P}\right)\cdot\frac{\left(1-\varepsilon\right)}{\varepsilon^3} \tag{13}$$

The first term, with a linear dependence on the gas velocity, is the laminar one, the second term is the turbulent one, with a quadratic dependence on gas velocity.

The equation can be written as function of the gas mass flow:

$$\frac{\Delta P}{L_i} = 150\left(\frac{\mu_{Gas}}{D_P^2 \cdot \rho_{Gas} \cdot S_i}\right) \cdot \frac{(1-\varepsilon)^2}{\varepsilon^3} \cdot g_i + \frac{7}{4} \cdot \left(\frac{1}{D_P \cdot \rho_{Gas} \cdot S_i^{\,2}}\right) \cdot \frac{(1-\varepsilon)}{\varepsilon^3} \cdot g_i^{\,2} \tag{14}$$

where the subscript *i* is referred to the east (*E*) and north (*N*) directions.

Finally, the energy conservation equation in the gaseous phase considers that CO and H_2 oxidation increases the temperature of gases in the cell; while mass transport, convection between solid and gas, and radiation between the gas in the cell and gas in neighboring ones are the main heat transfer mechanisms.

$$\begin{aligned} & c_{p\_Gas}(T_{Gas}) \cdot M_{Gas} \frac{dT_{Gas}}{dt} = g_{CO}(vl) \cdot HV_{CO} + HV_{H2} \cdot g_{H2} + \\ & g_{Gas\_in} \cdot c_{p\_Gas}(T_{Gas\_in}) \cdot T_{Gas\_in} - g_{Gas} \cdot c_{p\_Gas}(T_{Gas\_out}) \cdot T_{Gas\_out} + \\ & -\Gamma_{Gas\_Sol} \cdot S_{att} \cdot (T_{Gas} - T) + \lambda_{Gas\_RAD} \cdot \sum_{i=N,We} S_i \cdot \left(T_{Gas\_i}^{\,4} - T_{Gas}^{\,4}\right) + \\ & -\lambda_{Gas\_RAD} \cdot \sum_{i=E,S} S_i \cdot \left(T_{Gas}^{\,4} - T_{Gas\_i}^{\,4}\right) \end{aligned} \tag{15}$$

where $g_{CO(vl)}$ is the flow rate of CO due to the pyrolysis process; T_{GAS} is the temperature of the gas in the cell and T_{Gas_i} is the temperature of solid biomass in the cells next to the considered one.

5 Other plant components

Modelling approach for the other elements of the plant (the heat exchangers [26], the micro-turbine system [28, 29, 12], the ORC system) are well known in literature since are simply based on mass and energy balance equations as well as on the thermodynamic equations of the Brayton cycle, and on interpolation tests. They are reported here just for giving a complete view of the model.

5.1 Heat exchangers

Counter current gas flows and metallic walls to prevent gases mixing are the main characteristics of the heat exchanger in the plant (the gas-air exchanger, the recuperator and pre-heater). Due to the high temperature differences between gas/air inlet and outlet, the model of the heat exchanger is divided into cells. For each heat exchanger, the energy conservation equation (16) and the heat transfer equations (17-18) for gas/air on each side of the metallic walls are implemented [26].

$$W_{Gas} - W_a = M_m \cdot c_{p\_m} \cdot \frac{dT_m}{dt} \tag{16}$$

where W_{GAS} is the heat power from the hot gases to the process air and W_a is the heat power absorbed by the process air represented by the (17) and (18).

$$W_{Gas} = q_{Gas} \cdot c_{p\_Gas} \cdot (T_{Gas\_in} - T_{Gas\_out}) = S_{Gas\_m} \cdot \Gamma_{Gas\_m} \cdot \left(\frac{T_{Gas\_in} + T_{Gas\_out}}{2} - T_m\right) \tag{17}$$

$$W_a = q_a \cdot c_{p\_a} \cdot (T_{a\_out} - T_{a\_in}) = S_{a\_m} \cdot \Gamma_{a\_m} \cdot (T_m - \frac{T_{a\_in} + T_{a\_out}}{2}) \quad (18)$$

where S_{Gas_m} and S_{a_m} are the heat exchanger surfaces in contact with gas and process air respectively; Γ_{Gas_m} and Γ_{a_m} are the convective transfer coefficients between metal and gas or process air respectively.

5.2 Micro-turbine system

The micro-turbine system modelling is based on the physical model described in [28, 29] and also adopted in [12]. For the compressor, the air flow is a function of the rotational speed ω, the inlet air density ρ_a, and the dimensional characteristics of the machine (the parameter D_0 and the flow number Φ):

$$q_a = \Phi \cdot D_0^{\,3} \cdot \omega \cdot \rho_a \quad (19)$$

$\Phi\ D_0^3$ is defined as the ratio between the air flow and the nominal air density:

$$\Phi \cdot D_0^{\,3} = \frac{q_c}{\rho_{an}} \quad (20)$$

The air outlet temperature of the compressor is estimated assuming an isentropic compression in a perfect gas having $\gamma = c_p/c_v$ with compressor efficiency η_c (21), and the pressure ratio r_c:

$$T_{c\_out} = T_{c\_in} \cdot \left[1 + \frac{1}{\eta_c} \cdot \left(r_c^{\frac{\gamma-1}{\gamma}} - 1 \right) \right] \quad (21)$$

The mechanical power absorbed by the compressor is estimated as the product of the air flow rate and the enthalpy drop between compressor input and output:

$$W_c = q_c \cdot \left(h_{c\_out} - h_{c\_in} \right) = q_c \cdot \left(c_{p\_c\_out} \cdot T_{c\_out} - c_{p\_c\_in} \cdot T_{c\_in} \right) \quad (22)$$

The parameters γ e c_p depend upon temperature.

5.3 The turbine

The air flow rate of the turbine (q_{ex}) is estimated through the Stodola equation applied to the pressure drop between the turbine inlet and the system outlet.

$$q_{ex} = K_t \cdot P_{t\_in} \cdot \sqrt{\frac{1 - r_1}{T_{t\_in}}} \quad r_1 = \max\left(r_{cr}, \frac{P_{amb}}{P_{t\_in}} \right) \quad (23)$$

The critical value 0.5282 is the limit value for r_1 for a subcritical pressure drop, otherwise it is estimated as shown in (23).

The turbine exhaust pressure, used to estimate the expansion ratio, is assumed to be:

$$P_{ex} = P_a + k_0 \cdot \left(P_{t\_in} - P_{amb}\right) \tag{24}$$

458 to account for the share of pressure drop due to the heat exchangers that the exhausts cross before
459 the stack (k_0 is an appropriate constant).
460 The expansion ratio is defined as:

$$r_e = \frac{P_{ex}}{P_{t\_in}} \tag{25}$$

461 Turbine exhausts temperature is calculated according to (26):

$$T_{ex} = T_{t\_in} \cdot \left[1 + \eta_t \cdot \left(r_e^{\frac{\gamma-1}{\gamma}} - 1\right)\right] \tag{26}$$

462 The efficiency η_t changes as a function of the operating condition of the turbine, assuming the
463 maximum value at nominal conditions and decreasing according to a quadratic function of the ratio
464 $(\omega/\omega_n)/(\Delta h/\Delta h_n)$.
465 The mechanical power produced by the turbine is written as the product between the turbine air
466 flow rate and the enthalpy drop, considering the overall mechanical efficiency:

$$W_t = \eta_{mec} q_{ex} \left(h_{t\_in} - h_{ex}\right) = \eta_{mec} q_{ex} \left(c_{p\_t\_in} T_{t\_in} - c_{p\_ex} T_{ex}\right) \tag{27}$$

467 The net power is calculated as the difference between the power produced by the turbine and power
468 absorbed by the compressor.

$$W = W_t - W_c \tag{28}$$

469 This power is supposed to match the electric power generated since the dynamic behavior of the
470 electro-mechanic conversion system is one or two order of magnitude faster than the reminder of
471 the system.

472 5.4 The ORC system

473 The heat transfer processes dominate the dynamic behavior of the ORC system. It is therefore
474 simply modeled as a linear algebraic function of the temperature of the exhaust gas which is
475 composed by the process air coming from the recuperator and combustion gas from the pre-heater.
476 A time constant (10 minutes), estimated on the basis of the experimental tests, represents the inertia
477 of the system. Also the parameters of (29) have been derived by test and manufacturer data.

$$W_{ORC} = c_1 \cdot T_{ORC\_ex\_out} + c_2 \quad with \quad \begin{cases} c_1 = 0.27 K^{-1} \\ c_2 = -40.9 kW \end{cases} \tag{29}$$

478 The ORC model has not been tested and the overall system model has finally been used for simply
479 assessing the actual possibility of exploiting the ORC for increasing the electricity generation.
480 Characteristics of the system adopted in the pilot plant can be found in [6].

6 System tests and simulator validation

6.1 System performance

Measurements made on the EFMGT [5] used for test in the labs of the manufacturer, showed that the process air flowing through the heat exchanger has a mass flow of 0.7 kg/s and, during the steady state operation, is heated from 506°C up to 850°C. It means that 270 kW_t are transferred to the process air inside the heat generator. The micro-turbine efficiency, assessed as the ratio between this value and the net power output (70 kW_e) is therefore 25.9% [5].

Figure 6 shows the regenerative Brayton cycle curve of the micro-turbine system. The dashed lines describe the real compression and expansion, compared to the theoretical ones on the ideal cycle (solid curves).

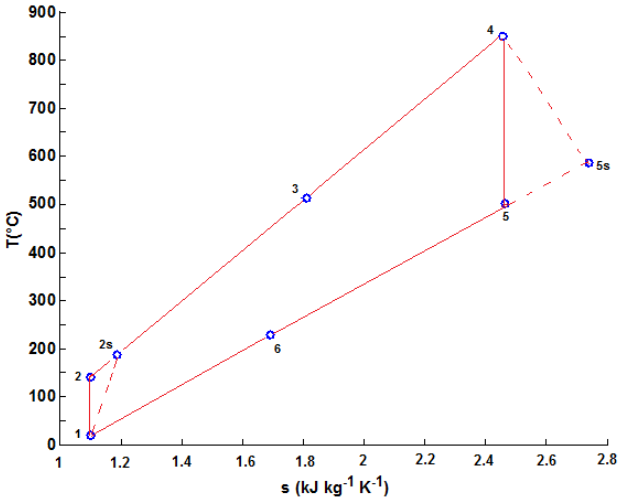

Figure 6: The regenerative Brayton cycle

The fuel used for the test was wood chip. A sample was characterized in the University labs and revealed 38.8% moisture content as a fraction of the whole mass and a Higher Heating Value of 17680 kJ/kg as well as a Lower Heating Value of 16880 kJ/kg for the dry material. A so wet fuel was used to completely check the model even in correctly accounting for the water evaporation process, which introduces a time delay between fuel supply and energy release.

The analysis of a sample of the fuel is reported in Table 2 and 3

Table 2: Analysis of the fuel

% (as received base)	Moisture	Volatiles	Fixed carbon	Ash
Pine chip	38.80	48.75	9.50	2.95

Table 3: Analysis of the fuel

% (dry base)	N	C	H	O	PCS (kJ/g)
Pine chip	0.36	45.84	5.57	43.41	17.68

Table 4 resumes the values of the density used in the simulator referred to equation (2). The content of water, char and ash have been slightly adapted in order to obtain the same thermal power for biomass at the entrance of the combustor, considering the reference biomass composition specified in section 4.1.

Table 4: Density of the biomass components

ρ_{Sol} [kg/m^3]	$\rho_C + ash$ [kg/m^3]	ρ_W [kg/m^3]	ρ_{vl1} [kg/m^3] (Tvl_1=250°C)	ρ_{vl2} [kg/m^3] (Tvl_2=350°C)	ρ_{vl3} [kg/m^3] (Tvl_3=550°C)
950	124	361	100	300	65

Concerning the overall efficiency, from biomass to electricity output, referring to the LHV and accounting for the heat spent for water evaporation (36.5 kW_t for 58 kg/h of water out of 150 kg/h of gross biomass), the useful heat during the tests was 395kW_t with a dry biomass flow 92 kg/h; hence the efficiency sums to 17.7%.

The heat generator exchange efficiency (given by the ratio between the heat supplied to the process air (270 kW_t) and fuel heat content) is therefore 68%.

Finally the useful heat which supplies the Rankine cycle is recovered from mixing the output from the turbine after the regenerative heat exchanger (0.68 kg/s @ 200°C) and the exhaust output from the heat generator (0.3 kg/s @ 420°C). The heat content referring to the system inlet temperature of 20°C is 250 kW_t. The power production of the ORC system increases the efficiency up to 23%.

6.2 Steady state calibration at rated condition

The simulator was validated at rated condition: 70 kW_e of net power production, 395 kW_t of biomass thermal power inlet at a 0.04 kg/s of flow rate. In this operating condition it has been possible to measure several variables in various points. Table 5 compares the main quantities measured along the system with those obtained by the simulator. The simulator results are very close to the experimental test; the maximum percentage deviation from the experimental values is about 5%. Uncertainty on experimental measurements has not been considered.

Table 5: Quantities measured along the system and results obtained by the simulator.

Measuring point	Experimental	Simulator	Deviation
Temperatures (°C) – process air			**% of the experimental values**
Compressor air inlet	21	21	0
Compressor air outlet	184	183	0.5
Heat exchanger air inlet	500	512	2.4
Turbine air inlet	850	855	0.6
Turbine air outlet	544	556	2.2
Recuperator outlet	200	210	5
Temperatures (°C) – Combustion air			**% of experimental values**
Combustor air inlet	1001	1012	1.1
Combustor air outlet	611	629	3
Pre-heater outlet	420	400	4.8
Air flow (kg/s) – process air			**% of experimental values**
--	0.68	0.65	4.4
Pressure ratio – process air			**% of experimental values**
--	3.9	3.75	3.8
Air flow (kg/s) – combustion air			**% of experimental values**
--	0.3	0.31	3.3

Gas-air heat exchanger temperature distribution, although estimated by a lumped parameter model, is very close to the real one; as the thermo graphic picture of figure 7 of the gas-air heat exchanger shows, the temperature of the heat-exchanger beams is uniform at 900°C in the front part, exposed to combustion gases radiation, while in the rear part, where convection is the main heat transfer mechanism, temperature reaches 600°C. Also in the simulator, the front part of the heat exchanger has a temperature of 905°C and 630°C in the rear part.

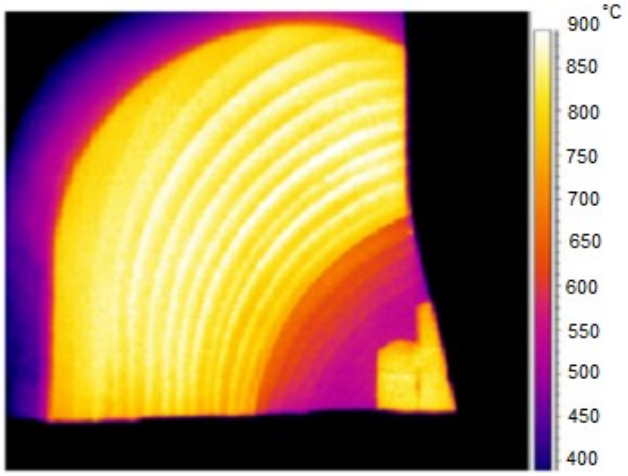

Figure 7: thermo graphic analysis on the gas-air heat exchanger.

6.3 Steady state validation at different operating points

In order to validate the simulator in different conditions for different biomass flows, figure 8 shows the net electric power as function of the turbine inlet temperature. The maximum difference between simulated and theoretical data is less than 5% from 800°C to 860°C, and 8% from 700°C to 800°C. This check enables considering that the thermodynamic model of the Brayton cycle is correctly modeled for what concerns energy balances. The dynamic of the gas turbine cycle is negligible compared to the time scales involved in combustion and heat transfer mechanism which are then checked with the dynamic test described in the next paragraph 6.4.

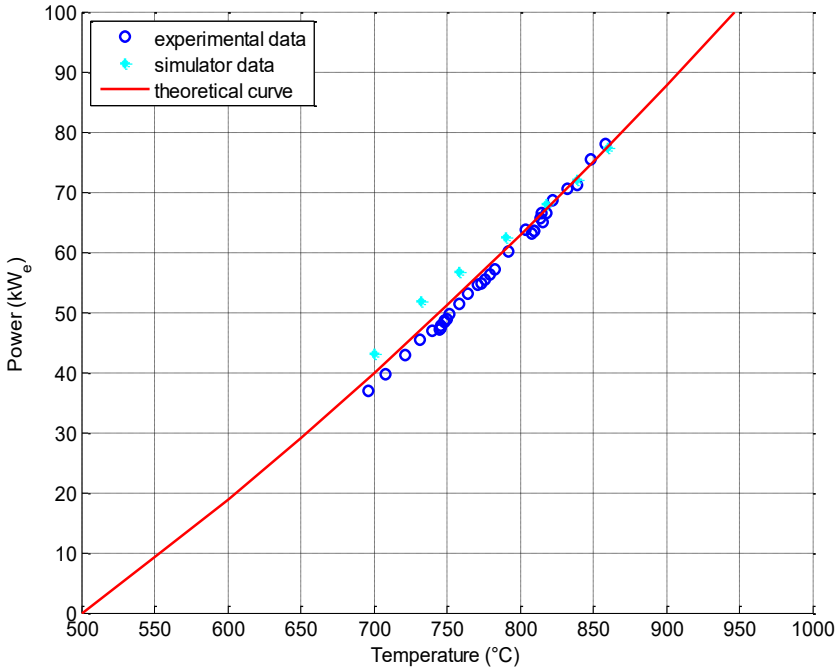

Figure 8: Net power vs. the turbine inlet temperature, theoretical values (red curve), experimental data (blue circles), estimated value (light blue dots).

6.4 Dynamic response and validation

The calibrated model has been checked by supposing to have the three air and biomass flow as shown in the first two graphs of figure 9. These data were recorded during a 500 minute test, including the starting transient, a first ramp to roughly 30kW, a second ramp up to 60kW and finally the sudden reduction down to 20kW. Primary, secondary and post combustion air have been estimated from the position of the vanes controlling the air flow. There is not a direct measure of air flow. Biomass flow is estimated from the supplying screw conveyor rotational speed. Vane positions and fuel flow were manually controlled during the test.

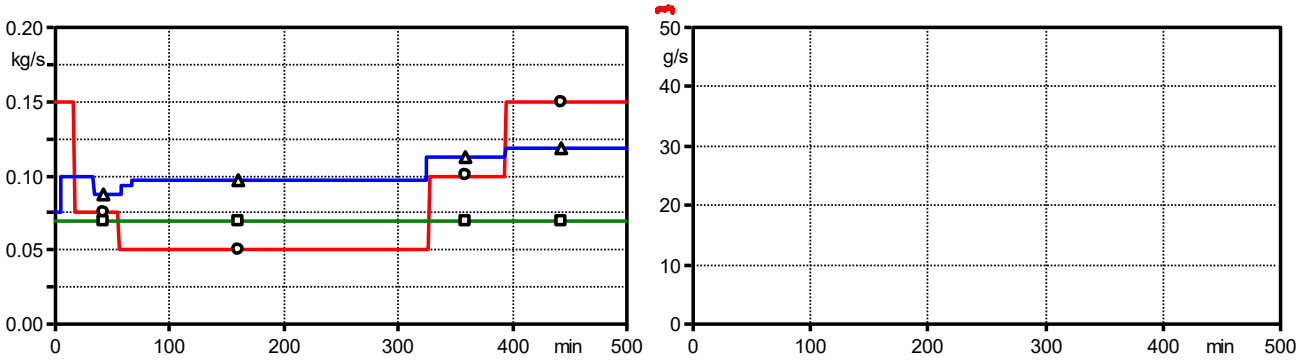

Air mass flow (primary: red and circle marks, secondary: green and square marks, post-combustion: blue and triangle marks)

Fuel mass flow

Figure 9: Input variables during dynamic tests

553 The comparison between the recorded values (shown in red and marked with circles) and the
554 simulated results (shown in green and marked with squares) is reported in the four graphs of figure
555 10.

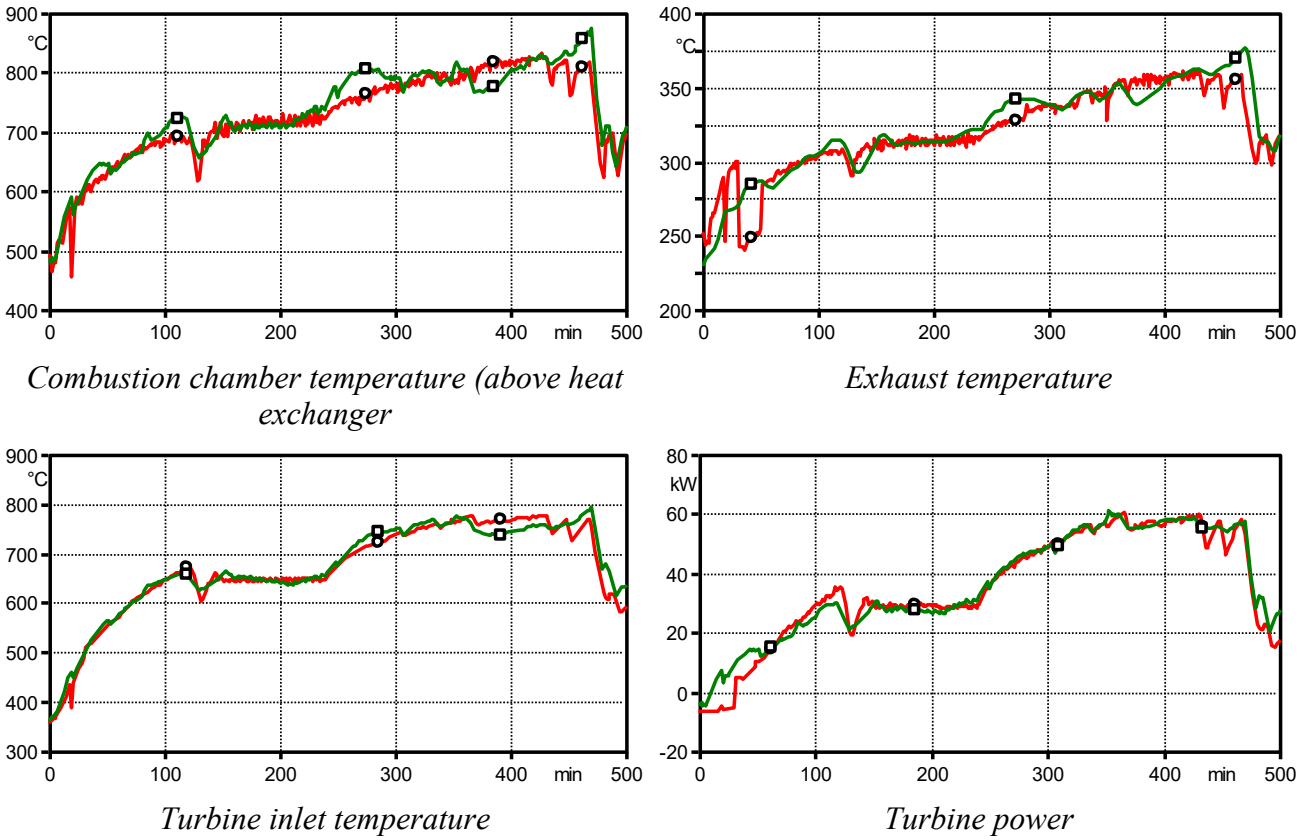

Combustion chamber temperature (above heat exchanger

Exhaust temperature

Turbine inlet temperature

Turbine power

Figure 10: Comparison between measured (red and circle marks) and simulated (green and square marks) variables

556 They show a good match of both the calculated instantaneous values and of the time constants
557 during the transient phases. There is a maximum instantaneous deviation of 50°C on the
558 temperature on the top of the combustion chamber which is a difficult to measure variable since
559 flame radiation affects the measurement. It is measured in a shielded position above the tubes of the

heat exchanger but it is not a reliable measurement in any case. The other two temperature values never show a deviation larger than 20°C. The result in term of power output never shows a mismatch larger than 5kW.

A detail of a transient representing a step change from 40 kW_e to 75 kW_e (gross values) is represented in figure 11. The power output from the simulator (the red and more stable curve) follows the experimental trend with a mean square error of 2.4% and shows a good match also of the dynamic time constant.

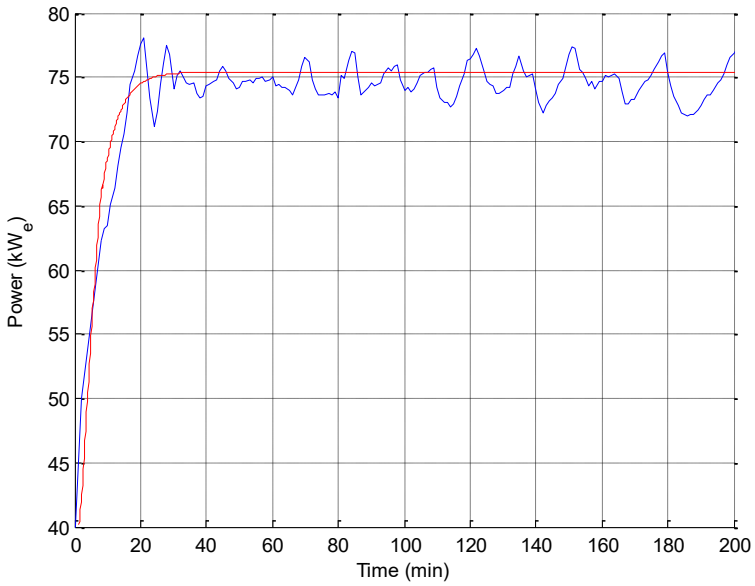

Figure 11: power before auxiliaries services vs. time, experimental data (blue and oscillating curve), simulator (red and steady curve).

7 Testing of a control system

The model was then used to test possible control schemes to regulate the profile that should be followed by the sum of the power produced by the EFMGT and the ORC. As shown in figure 12, an integral component ensures the total power produced by the system approaches the set-point value with a null steady state error. A *K* coefficient, less than one, depending upon the power produced by the ORC and the EFMGT, is an estimate of the power fraction coming from the EFMTG. The turbine controller converts the power set-point in the turbine inlet temperature set-point; a PI controller modulates the biomass flow and mutual proportion among the three inlets of combustion air, according to the turbine inlet temperature request. Protections ensure that the critical quantities don't exceed the technological limits.

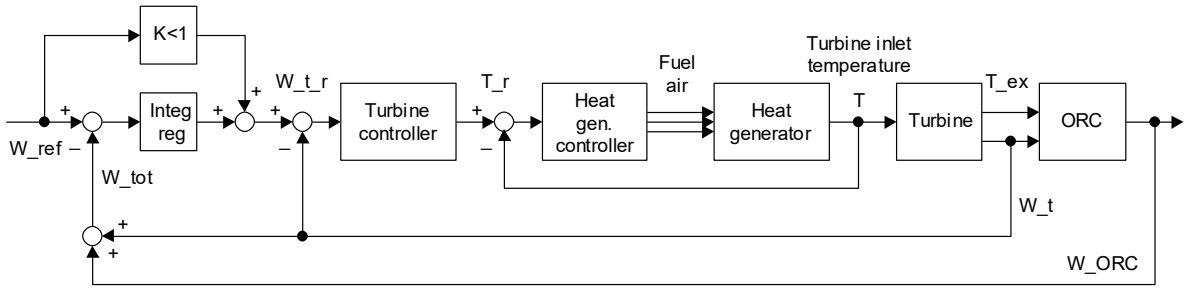

Figure 12: Block diagram of the control system.

A closed loop control is needed to make the system operate correctly when facing the continuous changing in the composition of biomass, i.e. in the heating value, the moisture content and the external temperature.

7.1 Controller response to power setpoint changes

The graph at the top of figure 13 shows the dynamic behaviour of the system, starting from nominal condition (105 kW_e), if a step from 105 kW_e to 15 kW_e and vice versa is requested.

EFMGT dynamic response is faster than the ORC due to the system inertia; the power production reaches 15 kW_e after 40 minutes from the request. In this condition, the exhaust temperature is too low to warm the organic fluid and no power is produced by the ORC. 40 minutes are necessary to reach the nominal condition again. It's worth remarking that the EFMGT changes its regime in 15 minutes.

The second and the third graphs of figure 13 show biomass and combustion air flow rate; biomass flow rate reaches his minimum value when the minimum power production is imposed, then a constant value of 0.02 kg/s is reached for 15 kW_e of power production. When the rated value of power production of 105 kW_e is imposed again, the biomass flow rate reaches its nominal value of 0.04 kg/s after a transient overshoot up to 0.06 kg/s, which is the maximum conveyor flow.

Total combustion air is supposed to stay at a constant value (sum of primary, secondary and post-combustion air); also post-combustion air is a constant value in order to ensure the right dilution of exhaust gas.

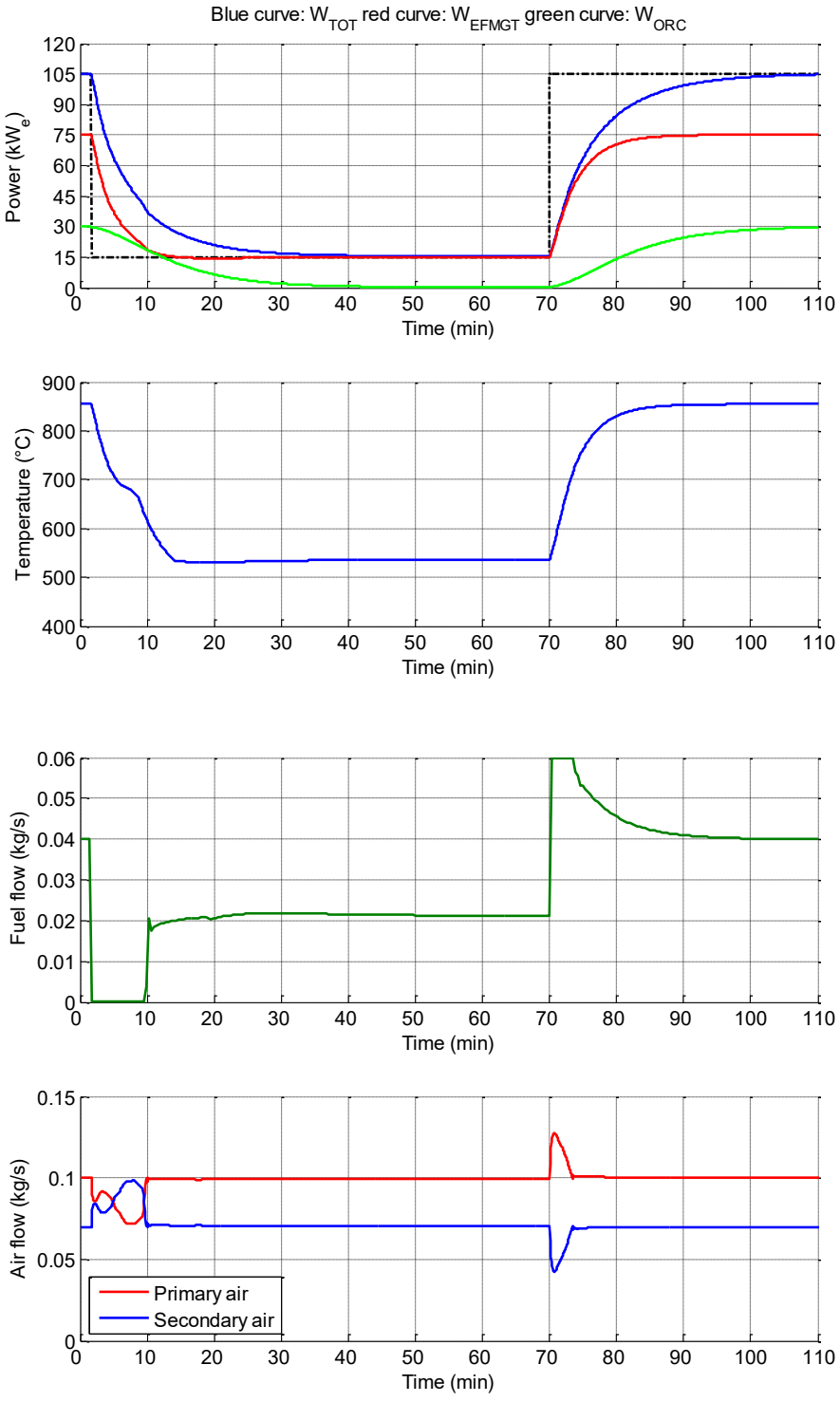

Figure 13: dynamic behaviour of the system (electric power, turbine inlet temperature, fuel flow and air flow vs. time) after power set point change: from nominal condition (105 kW_e) to minimum power (15 kW_e) and to nominal condition (105 kW_e).

7.2 Controller response to biomass moisture change

If the moisture content abruptly changes due to switching to a different storage, the inlet turbine temperature changes as well. The control system is able to restore the nominal conditions by adapting the biomass flow rate.

In order to show this effect, two step changes in the biomass moisture content (from 30% to 38% and then vice-versa) were imposed during the plant operation starting from rated and steady operating conditions and without any controller in service: fuel mass flow, as well as air flow remain at a constant level. The initial rated operating conditions have different fuel and air flow values if compared to figure 13 where the biomass moisture content was 38% (matching the experimental conditions).

Figure 14 shows the power production and the turbine inlet temperature behaviors during the transient. The turbine inlet temperature decreases from about 860°C to 800°C after the first step, and the total electrical power produced by the plant, consequently decreases from 105 kW_e to 90 kW_e as well as the electrical power produced by the EFMGT and ORC decrease too. The second step (from 38% to 30% at 200 minutes) restores the nominal conditions.

Obviously, without the controller operation, the fuel, primary air and secondary air flow rates are constant to the initial value.

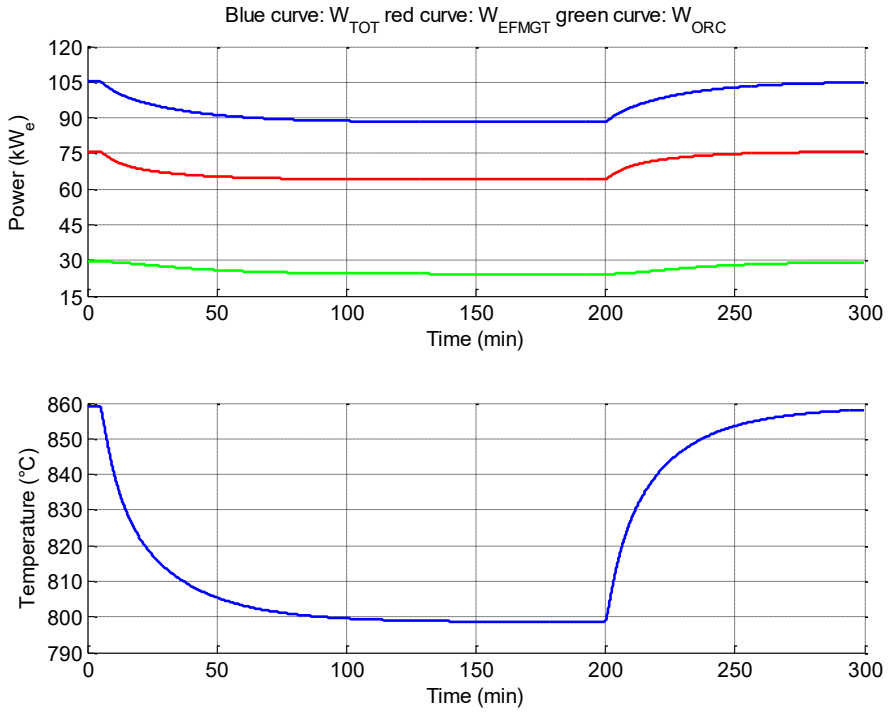

Figure 14: power production and turbine inlet temperature after a moisture content changing (from 30% to 38% and from 38% to 30%).

The same transient was then simulated with the controller in service (figure 15). The same disturbance regarding the biomass moisture content (from 30% to 38%), does not produce any effect on the turbine inlet temperature and the electrical power produced by the plant: the controller acts on the fuel flow rate (from 0.035 kg/s to about 0.038 kg/s) in order to keep the plant performances unchanged. The primary and secondary air flow rates remain constant since the amount of dry biomass roughly does not change.

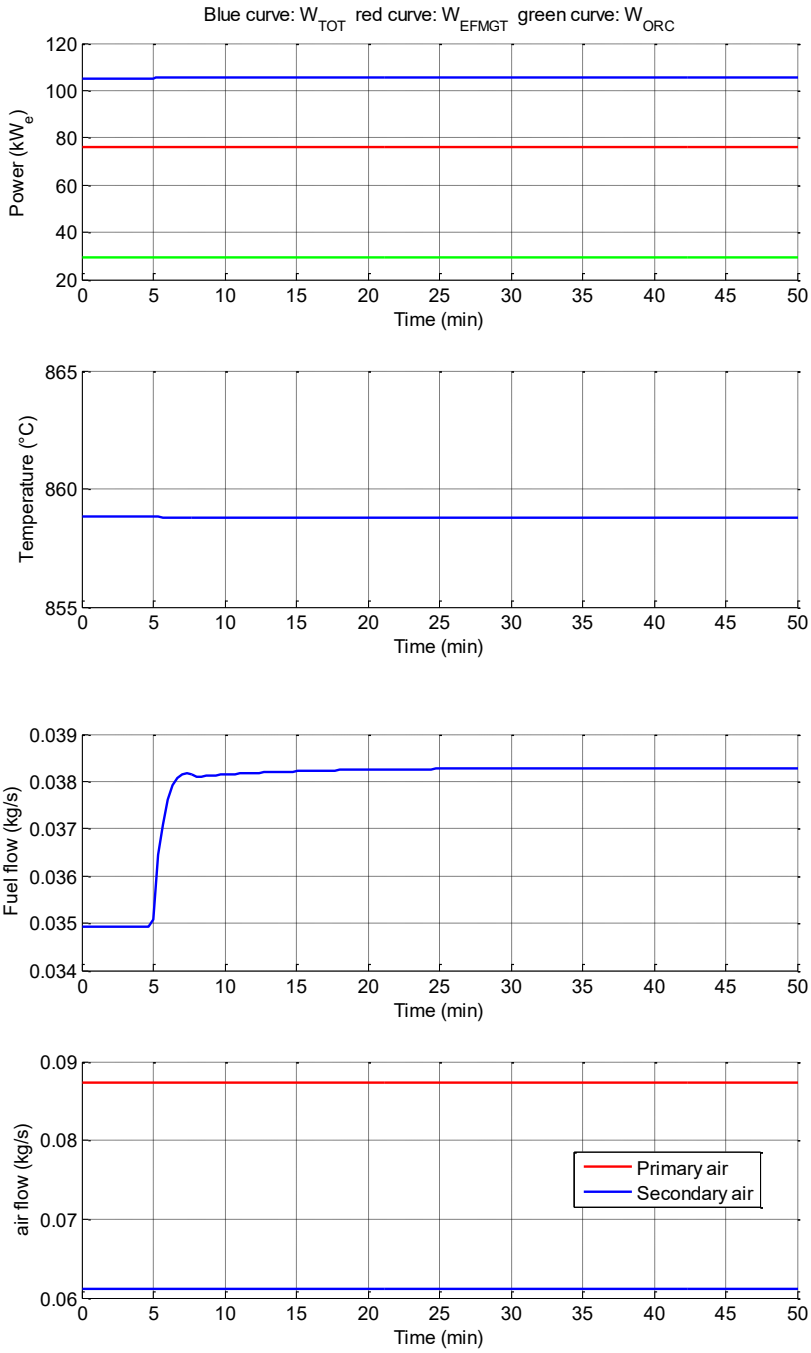

Figure 15: power production, turbine inlet temperature and biomass and air flow rates after a moisture content changing (from 30% to 38%).

8 Conclusions

The growing interest in biomass energy utilization needs to develop appropriate instruments to study the behaviour of systems which exploit this renewable source.

An effective simulator, able to reproduce a realistic dynamic behaviour of a biomass power plant has been developed.

The mathematical model is based on the description of the main physical phenomena that involve the combustion process, the heat exchanger mechanisms and the power production.

The simulator was fit on an externally fired micro gas turbine (EFMGT) system, supplying 70 kW of electricity and based on biomass combustion, but can be easily adapted to other systems based on the same principle.

Despite a not detailed characterization of the system, the approach based on the physical principles highlights the mechanisms and parameters that more affect the system performances and behaviour. The main the results of the simulations are very close to experimental ones. At rated steady state conditions differences in the main variables are all below 5%. During transient operation the main temperatures affecting the system performance differ from the measured values less than 20°C and the power produced less than 5kW. As a consequence, the model, which the simulator is based on, was a successful instrument to test a possible control scheme.

Concluding, the simulator combines two modelling approaches, the first oriented to provide a reliable system behaviour representation, the second oriented to system control issues to design an effective control in various operating conditions and so improve its performance in power production.

Bibliography

[1] C. Caputo, M. Palumbo, P.M. Pelagagge, F. Schacchia: "Economics of biomass energy utilization in combustion and gasification plants: effects of logistic variables", Biomass & Bioenergy, Volume 28, Pages 35-51, 2005.

[2] P. McKendry: "Energy production from biomass (part 2): conversion technologies" Bioresource Technology, Volume 83, Pages 47–54, 2002.

[3] M. Kautz, U. Hansen: "The externally fired gas turbine (EFGT-cycle) for decentralised use of biomass", Applied Energy, Volume 84, Issues 7-8, July-August 2007, Pages 795-805.

[4] S. Carrara: "Small-scale biomass power generation" Ph.D. Thesis, University of Bergamo, 2010.

[5] S. Barsali, R. Giglioli. D. Poli., "An externally fired micro gas turbine plant for combined heat and power generation from solid biomass: a practical experience" Proc. 18th European Biomass Conference and Exhibition, Lyon, 2010

[6] M. Barcaglioni, S. Barsali, R. Giglioli, G. Ludovici, D. Poli: "A micro combined cycle plant for power generation from solid biomass: coupling EFMGT e ORC," Proc. 19th European Biomass Conference and Exhibition, Berlin, 2011.

[7] K.L. Chien, E.I. Ergin, A. Lee, C. Ling:"Dynamic analysis of a boiler", Trans. ASME, Volume 80, Pages 1809–1819, 1958.

[8] E. Eitelberg , J. Franke , G.K Lausterer: “Modular modelling applied to a Benson boiler”, in 1st IFAC workshop on Modelling and Control of Electric Power Plants, Como, 1983.

[9] C. Maffezzoni: “Issues in modelling and simulation of power plants”, Proc. IFAC Symposium. on Control of Power Plants and Power Systems, Munich, 1, 19–27, 1992.

[10] A. Leva, C. Maffezzoni: “Modelling of power plants”, in D. Flynn (Ed.), “Thermal power plant simulation and control”, IEE, London, 17–60, 2003.

[11] K.J. Astrom, R.D. Bell: “A non-linear model for steam generation process”, Prepr. 12th IFAC World Congress, Sydney,Volume 3, 395–398, 1993.

[12] S. Barsali, A. De Marco, G. M. Giannuzzi, F. Mazzoldi, A. Possenti and R. Zaottini: “Modeling combined cycle power plants for power system restoration studies” IEEE Transactions on Energy Conversion Volume 27, Issue 2, June 2012, pages 340-350

[13] V. Máša, M. Pavlas, I. Švarc: “Mathematical model of biomass boiler for control purposes”, Chemical Engineering Transactions, Volume 25, Pages 743-748, 2011.

[14] A. Cano, J. Carpio, F. Jurado: “Modelling of combined cycle power plants using biomass”, Renewable Energy, Volume 28, Pages 743–753, 2003.

[15] D. Hainsworth, J.M. Jones, M. Pourkashanian, A. Williams: “A comprehensive biomass combustion model”, Renewable Energy, Volume 19, Pages. 229-234, 2000.

[16] A. Friedl , M. Harasek, A. Makaruk, M. Miltner:. "CFD modelling for the combustion of solid baled biomass," in Fifth International Conference on CFD in the Process Industries CSIRO, Melbourne,Pages 13-15, 2006.

[17] S. Clausen, T. Hille, S. L. Hvid, S. K. Kær, L. Rosendahl , C. Yin: “Mathematical modeling and experimental study of biomass combustion in a thermal 108 MW grate-fired boiler”, Energy & Fuels, Volume. 22, Pages 1380–1390, 2008.

[18] F. Casella, A. Leva: “Modelica open library for power plant simulation: design and experimental validation”, Proc. of the 3rd International Modelica Conference, Linköping, Pages 41-50, 2003.

[19] M. Barcaglioni, S. Barsali, R. Giglioli, G. Ludovici, D. Poli: “Field tests on a new micro combined cycle plant based on EFMGT and ORC”, Proc. 20th European Biomass Conference and Exhibition, Milan, 2012.

[20] C.A. Koufopanos, A. Lucchesi, G. Maschio: “Kinetic modeling of the pyrolysis of biomass and biomass components”, The Canadian Journal of Chemical Enginireeing, Volume 67, p. 75–84, 1989.

[21] C. Di Blasi: “Modeling chemical and physical processes of wood and biomass pyrolysis”, Progress in Energy and Combustion Science, Volume. 34, Pages 47–90, 2008.

[22] C. Di Blasi: “Combustion and gasification rates of lignocellulosic chars”, Progress in Energy and Combustion Science, Volume. 35, Pages 121–140, 2009

[23] H. C. Williams, A. Hottel, N. M. Nerhein, G. R. Schneider, “Kinetic studies in stirred reactors: combustion of carbon monoxide and propane”, Tenth Symposium (International) on Combustion, The combustion institute, Pittsburgh, 111, 1965.

[24] M. E. Prah, H. Hofbauer, F.Winter: “Temperatures in a fuel particle burning in a fluidized bed: the effect of drying, devolatilization, and char combustion”, Combustion and flame, Volume 108, no. 3, Pages 302-314, 1997.

[25] P. Basu, “Combustion of a coal in circulating fluidizad-bed boilers: a review”, Chemical Engineering Science, no. 54, Pages 5547-5557, 1999.

[26] F. Kreith, R.M. Manglik, M.S. Bohn “Principles of Heat Transfer” Brooks/Cole USA, 2010

[27] R. B. Bird, E. Stuart, E. N. Lightfoot: “Transport phenomena”, 2nd Edition, Pages 188-192 (6.4-12).

[28] S. L .Dixon, “Fluid mechanics and thermodynamics of turbomachinery”, Burlington: Elsevier Butterworth-Heinemann, 2005

[29] A. De Marco: “Modelli matematici di turbogas e confronto con prove sperimentali”, 94a Riunione annuale AEI, Ancona, 3-6 Ottobre 1993.

[30] Perry's Chemical Engineers' Handbook, Eighth Edition Hardcover – November 13, 2007

[31] L. Devi, K.J. Ptasinski, F.J.J.G. Janssen, “A review of the primary measures for tar elimination in biomass gasification processes”, Biomass and Bioenergy, 24, 2003, pp. 125–140.

[32] C. Li, K. Suzuki, “Tar property, analysis, reforming mechanism and model for biomass gasification - An overview”, Renewable and Sustainable Energy Reviews, 13, 2009, pp. 594-604.